A Pipeline for Topology Optimization of Reinforced Concrete Frames: A Systematic Approach for Ground Structure Generation, Selection and Optimization

Yohannes L. Alemu *, Bedilu Habte , Girum Urgessa , Christian Walther , Tom Lahmer

Posted Date: 3 April 2026

doi: 10.20944/preprints202604.0258.v1

Keywords: topology optimization pipeline; reinforced concrete frame ground structure; graph-based Latin Hypercube Sampling; sparse gaussian process surrogate model; Compliance Prediction Map; Reinforced Concrete Frame Topology Optimization

 doi:10.20944/preprints202604.0258.v1

Article

A Pipeline for Topology Optimization of Reinforced Concrete Frames: A Systematic Approach for Ground Structure Generation, Selection and Optimization

Yohannes L. Alemu [1,*], Bedilu Habte [2], Girum Urgessa [3], Christian Walther [1] and Tom Lahmer [1]

[1] Institute of Structural Mechanics, Bauhaus University, Germany
[2] School of Civil and Environmental Engineering, Addis Ababa Institute of Technology, Ethiopia
[3] Department of Civil and Environmental Engineering, College of Engineering and Architecture, Howard University, Washington, DC 20059, USA
* Correspondence: yohannes.lisanework.alemu@uni-weimar.de

Abstract

The topology optimization of reinforced concrete (RC) building frames is relatively underexplored compared to steel structures, partly due to the lack of a systematic approach to generate and select ground structures (GS). Existing methods often use less systematic GS strategies, limiting efficient exploration of the vast and sparse design space shaped by large bay widths and story heights. This work addresses this gap by providing a comprehensive and systematic pipeline tailored for RC frames. The key contributions are: (1) development of a GS generation framework that systematically enumerates all feasible RC frame configurations within user-defined constraints, (2) introduction of a candidate GS selection map, a surrogate-based tool employing graph-based Latin Hypercube Sampling (LHS) and sparse Gaussian Process (GP) models, which predicts compliance early and strategically guides candidate selection, significantly reducing computational cost while serving as a reference for understanding design parameter influences; and (3) implementation of an integrated topology optimization pipeline applying particle swarm optimization (PSO) to selected candidates, achieving efficient compliance minimization with reduced computational effort. The complete workflow - which spans GS generation, surrogate-based candidate selection, and iterative optimization - is implemented and validated in two design domains with width-to-height aspect ratios of 1:1 and 1:1.5 and generates 438,984 and 104,032 different frame configurations respectively. The selected candidates undergo PSO-based optimization, yielding designs with volume fractions below 0.55 and preserving critical floor beams, demonstrating the framework's ability to enable the design of structurally efficient RC frames. The framework is designed to be extensible, with direct applicability to broader RC design scenarios including three-dimensional frames and nonlinear analysis in future work.

Keywords: topology optimization pipeline; reinforced concrete frame ground structure; graph-based Latin Hypercube Sampling; sparse gaussian process surrogate model; Compliance Prediction Map; Reinforced Concrete Frame Topology Optimization

1. Introduction

Topology optimization seeks to determine the most efficient material distribution within a predefined design domain, subject to applied loads, boundary conditions, and specific performance criteria. The nature of the objective function plays a central role in shaping the optimal structure. Two known objective formulations are stress minimization and compliance minimization, each producing distinct structural layouts and serving different engineering priorities.

Stress minimization focuses on limiting material stresses to remain within allowable limits, resulting in designs that are typically more redundant, with multiple load paths. This often results in structures composed of many slender members. While beneficial for robustness and reliability;

 doi:10.20944/preprints202604.0258.v1

especially in structures where multiple load paths are desirable, the stress-based approach is computationally intensive due to the complexity of satisfying local stress constraints in iterative design updates.

Compliance minimization, in contrast, aims to reduce the total strain energy or equivalently maximize global stiffness. This method tends to produce fewer structural members with larger cross-sectional areas, leading to more efficient yet sparse structural configurations. Compliance-based designs are computationally simpler and more scalable, making them a popular choice in practical applications. From the perspective of reinforced concrete (RC) structures, compliance minimization is often more suitable. RC members are subject to constructability constraints such as minimum cross-sectional dimensions required to accommodate reinforcement and concrete aggregate. Therefore, a design that favors fewer, thicker members aligns better with real-world RC detailing requirements. On the other hand, for frame-type or steel structures where member slenderness is more acceptable and structural redundancy is desirable, stress-based formulations may be preferred despite their higher computational cost.

Topology optimization of structures with a continuum domain start with a solid surface or volumetric object as the approach is density-based. For discrete structures, which are mainly framed, however, the ground structure is used. A ground structure serves as a starting structure for an optimization task, where iterative adjustments are made to its members and topology to achieve an optimal structure [1]. Due to the significant influence of node positions and the number of connected members on the initial ground structure, various studies have been conducted to address both computational burden and optimality [2–4].

A fully connected ground structure, in which every node is connected to every other node by all possible connections, leads to a complex optimization process and requires significant computational resources, including considerable computer capacity and time [5]. Overlapping members, inclusion of slender members, and structural instability pose challenges to overcome when contemplating such a ground structure[6].

A second approach is addressed in various ways, such as gradually removing unfit members and adding fit members, or generating levels of connectivity to include the preferred number of members based on the required solution accuracy[7–9].

Ranalli, et al. [10] employed a foundational framework to reduce the overall installed expenses of steel frame structures. Sequentially, they implemented topology and size optimizations as outer and inner loops. Sokol [5] utilized a foundational structure for conducting topology optimization of large-scale trusses. His methodology began by prioritizing shorter member-to-node connections and gradually incorporated longer potential members. Following his approach, as new members were potentially added, less-critical existing members were removed.

The aforementioned approaches, however, have not been further extended to RC structures due to the orthogonal orientation of member connectivity. Reinforced concrete structures have undoubtedly earned significant attention in the research community, both as reinforced concrete [11–13] and composed of structural steel [14,15], indicating that such optimization is of great importance.

2. Motivation and Structure

Reinforced concrete (RC) building frames typically exhibit relatively sparse connectivity, yet the number of potential frame configurations within a given spatial domain can be extremely large. This arises from combinatorial variations in node placement, bay width, and story height parameters that are bounded by constructional constraints but still allow for a vast number of feasible layouts. Such complexity calls for a systematic and efficient approach to generating and selecting candidate ground structures suitable for topology optimization, particularly because the optimization process involves repeated structural reanalysis and is computationally demanding. The scarcity of research that explicitly addresses this challenge within the context of RC frames further highlights the need for a targeted methodology.

 doi:10.20944/preprints202604.0258.v1

Conventional ground structure-based topology optimization approaches generally begin with a single predefined frame and seek to optimize member connectivity within that fixed layout. Whether fully connected (where all nodes are linked), neighbor-based (where connections are restricted to adjacent nodes), or growth-based (where elements are progressively added during optimization), these methods share a core limitation: they operate within the confines of one initial ground structure. As a result, they are inherently unable to capture the full diversity of frame configurations permitted by RC design constraints, such as minimum bay width and story height. This restricts their ability to explore realistic yet diverse structural possibilities.

The approach proposed in this work addresses this limitation by systematically enumerating all feasible RC frame configurations over a given domain, subject to geometric and constructional constraints. Each configuration yields a distinct, sparse, and structurally meaningful ground structure.

This work addresses the challenge by proposing a structured methodology for generating and optimizing RC frame configurations. The remainder of the paper is organized as follows:

- Section 3 introduces a systematic ground structure generation method,
- Section 4 outlines the overall methodological framework,
- Section 5 presents the compliance minimization formulation and its optimization requirements,
- Section 6 explores the use of surrogate models for rapid compliance prediction to support candidate selection,
- Section 7 applies full topology optimization to the selected candidate structures,
- Finally, the Conclusion section discusses implications and future directions.

3. Enumerative RC Frame Ground Structure Generation

This section presents how all possible RC frames could be generated within a given frame domain and considerable constraints. This corresponds to each set of nodal location interval. Hence, for multiple nodal intervals, there will be a larger set of all possible frames which are stored under each nodal location interval as a subset. Contrasted to the existing approaches, which connects all nodes and throw it to the optimization, this approach allows only meaningful nodal connectivity for each frame.

Given a domain space and bay-width and story height bounds, all possible nodes are first generated. Each set of nodal location intervals along the existing axes returns different set of frames. Basic ground structure frame, formed by connecting nodes orthogonally, is generated for each set of nodes.

3.1. Nodes

Given a $W \times H$ frame domain, where:

The allowable dimensions for bays and stories are defined by:

$$\begin{aligned} \mathcal{W} &= \{w_i \mid w_{\min} \leq w_i \leq w_{\max}\}, \\ \mathcal{H} &= \{h_j \mid h_{\min} \leq h_j \leq h_{\max}\}. \end{aligned} \tag{1}$$

where:

- $\mathcal{W}$ Set of allowable bay widths,
- $\mathcal{H}$ Set of allowable story heights,
- w_i Width of the i^{th} bay option,
- h_j Height of the j^{th} story option.

For given nodal location intervals w_{int} and h_{int}, discrete nodal locations are defined within the frame domain while generating nodes for multiple different sets of frames. Accordingly, bay sequences and story sequences are generated.

 doi:10.20944/preprints202604.0258.v1

3.1.1. Bay Sequences

$$\mathcal{B} = \left\{ \mathbf{B} = (b_1, \ldots, b_{N_b}) \mid b_k \in \mathcal{W}, \quad W_{\max} - w_{\min} \leq \sum_{k=1}^{N_b} b_k \leq W_{\max} \right\}. \tag{2}$$

where:

$\mathbf{B}$	Sequence of bay widths,
b_k	Width of the k^{th} bay,
N_b	Number of bays,
$W_{\max}$	Maximum total domain width,
$w_{\min}$	Minimum allowable bay width.

3.1.2. Story Sequences

$$\mathcal{S} = \left\{ \mathbf{S} = (s_1, \ldots, s_{N_s}) \mid s_l \in \mathcal{H}, \quad H_{\max} - h_{\min} \leq \sum_{l=1}^{N_s} s_l \leq H_{\max} \right\}. \tag{3}$$

where:

$\mathbf{S}$	Sequence of story heights,
s_l	Height of the l^{th} story,
N_s	Number of stories,
$H_{\max}$	Maximum total domain height,
$h_{\min}$	Minimum allowable story height.

3.1.3. Nodal Grid Generation

Each nodal grid $\mathcal{N}(\mathbf{B}, \mathbf{S})$ is defined by the cumulative positions of bays and stories:

$$x_i = \sum_{k=1}^{i-1} b_k, \quad i = 1, \ldots, N_b + 1,$$

$$y_j = \sum_{l=1}^{j-1} s_l, \quad j = 1, \ldots, N_s + 1,$$

$$\mathcal{G} = \{ \mathcal{N}(\mathbf{B}, \mathbf{S}) \mid \mathbf{B} \in \mathcal{B}, \quad \mathbf{S} \in \mathcal{S} \}. \tag{4}$$

where:

$\mathcal{G}$	Set of all feasible nodal grids,
$\mathcal{N}(\mathbf{B}, \mathbf{S})$	Nodal grid from bay and story sequences,
x_i	Horizontal position of grid line i,
y_j	Vertical position of grid line j.

3.1.4. Number of Nodes

$$N_{\text{nodes}} = (N_b + 1)(N_s + 1). \tag{5}$$

where:

N_{nodes}	Total number of nodal intersections in the 2D grid.

3.1.5. Perturbable Node Set

In order to keep area of a slab unaffected, edge nodes should be excluded from perturbation. Moreover, base nodes are also excluded so as to avoid that ground structure (GS) from being changed

 doi:10.20944/preprints202604.0258.v1

to another GS in another configuration. Still to keep floor area unaffected, the nodes that are allowed to perturb horizontally exclude:

- Nodes on the leftmost vertical axis ($i = 0$),
- Nodes on the rightmost vertical axis ($i = N_b$),
- Nodes on the bottommost horizontal axis ($j = 0$).

Thus, the set of perturbable nodes is as follows:

$$\mathcal{P} = \{(i, j) \mid i = 1, \ldots, N_b - 1, \quad j = 1, \ldots, N_s\}. \tag{6}$$

3.1.6. Bay Width Constraint Under Perturbation

To ensure valid configurations under perturbation:

$$w_{\min} \leq b_k \leq w_{\max}. \tag{7}$$

Let δ be the magnitude of the horizontal perturbation. A node $(i, j) \in \mathcal{P}$ can:

- Move left by δ if both b_{i-1} and b_i remain within bounds,
- Move right by δ under the same condition,
- Or remain in place.

Figure 1a shows all nodes generated for a given pair of bay width and story height interval ranges. Subsets of these nodes connect to result in large number of possible frames. For a $[w_{min}, w_{max}]$ bay width bound of $[3m, 7m]$ and a $[h_{min}, h_{max}]$ story height bound $[2.8m, 4m]$ and $10m$ by $10m$ domain size, and an interval range of $0.5m$ for both bay width and story height used, and also a δ $0.2m$ lateral nodal perturbation is allowed, 26208 ground structures that result in a total of 438984 frames (both perturbed and normal) are generated. Regardless of the connectivity level, for each chosen connectivity level such number of frames is generated. This is because the number of frames is decided based on level 1 connectivity and perturbation. The rest levels change only the connectivities of these resulted frames. Variation in the interval range correspond to the fineness or coarseness of mesh grids in the mesh grid approach. Smaller interval ranges produce nearly similar frames. One of the top interior nodes is perturbed to the right on Figure 1d,f.

3.2. Elements

The connectivity levels are built on top of basic GS connectivity, which connects nodes orthogonally as seen on Figure 1b. The connectivity levels therefore, dictate the diagonal nodal connectivity.

Level 1 connectivity is defined by linking nodes within the same bay-story box via immediate diagonal connections along the frame axes.

Level 2 connectivity extends this by allowing diagonal connections to nodes in the adjacent bay-story boxes in all directions within the plane, effectively permitting each node to connect within a 3×3 nodal grid. This level captures more complex interactions and increases the design space.

Perturbed Level 1 connectivity is formed by allowing perturbation of node/s laterally on each of the frames generated with Level 1 connectivity. When nodes are perturbed, this allows for the emergence of inclined members, enabling a more versatile structural layout.

Perturbed Level 2 connectivity is formed by allowing perturbation of node/s laterally on each of the frames generated with Level 2 connectivity.

The proposed ground structure generation method captures all possible connections for the resolution defined by the selected nodal location interval. Topology optimization can be applied to structures with Level 1, Level 2, or higher levels of connectivity, including fully connected frames. However, in reinforced concrete (RC) framed structures—where members cannot be made as small as in steel frames—excessive connectivity may lead to element congestion, slenderness issues, and increased construction complexity. As such, limiting connectivity to Level 2 could generally be more

 doi:10.20944/preprints202604.0258.v1

appropriate and practical for RC frames. Moreover, elements for above level 1 connectivity consider removal of longer elements based on proximity among them measured in degrees.

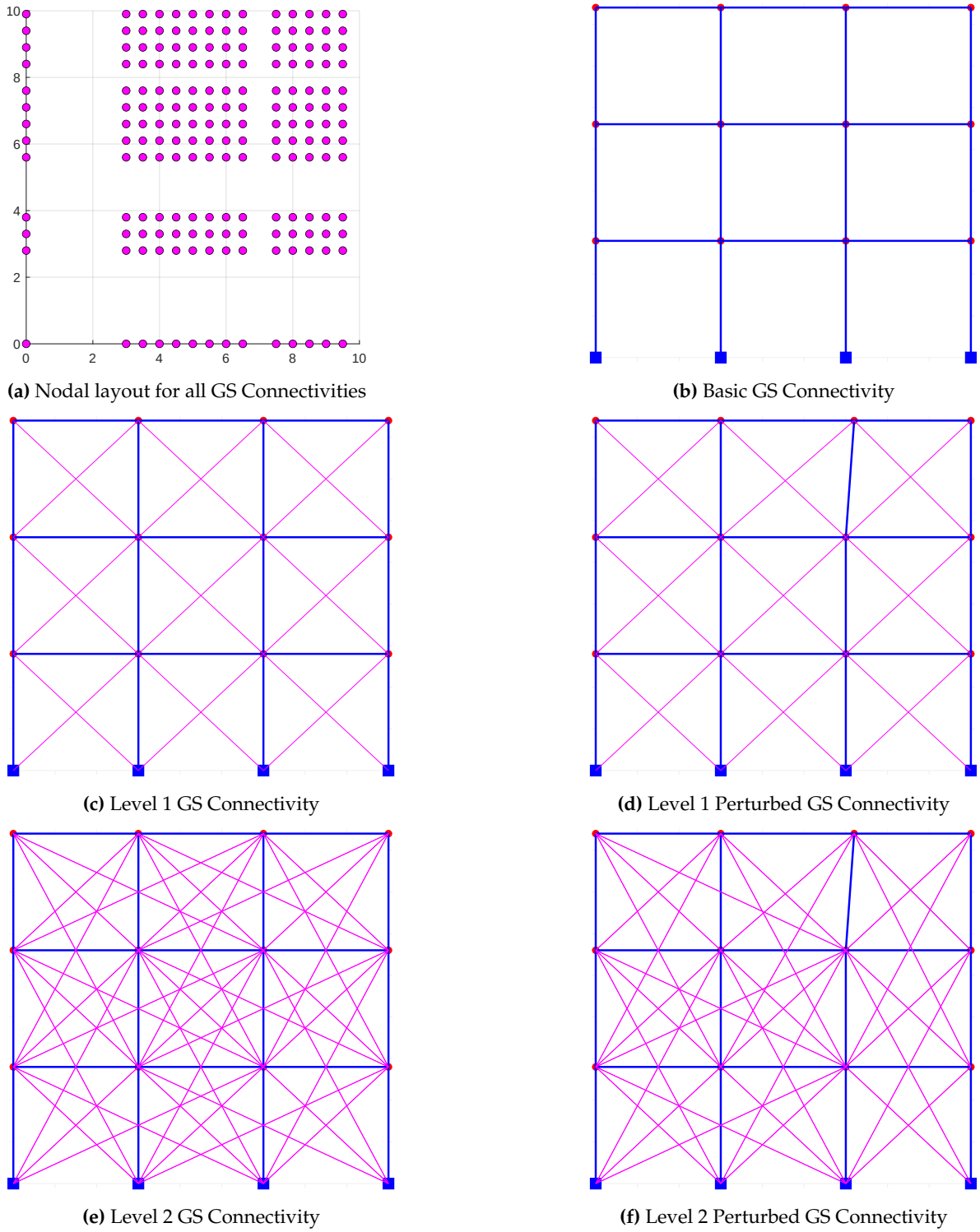

(a) Nodal layout for all GS Connectivities

(b) Basic GS Connectivity

(c) Level 1 GS Connectivity

(d) Level 1 Perturbed GS Connectivity

(e) Level 2 GS Connectivity

(f) Level 2 Perturbed GS Connectivity

Figure 1. Node Generation and Element Connectivity of 2D Frames.

For 2D case the total number of elements E_{2D} for level 1 connectivity is given by:

$$E_{2D} = N_b N_s + (N_b + 1)N_s + 2N_b N_s. \tag{8}$$

The first, second, and third components of the summation represent the number of beam, column, and diagonal elements, respectively.

 doi:10.20944/preprints202604.0258.v1

3.3. Frames

The total number of frames is calculated below as N_{layouts}.
Let $p_{i,j} \in \{1, 2, 3\}$ denote the number of valid perturbation options at node (i, j). Then:

$$N_{\text{layouts}} = \prod_{(i,j)\in\mathcal{P}} p_{i,j}. \tag{9}$$

where:

N_b, N_s	Number of bays and stories,
$\mathcal{P}$	Set of perturbable node indices,
b_k	Width of the k^{th} bay,
δ	Perturbation magnitude,
$p_{i,j}$	Valid perturbation options at node (i, j),
N_{layouts}	Total number of unique perturbed layouts.

4. Methodology

4.1. Reinforced Concrete Material Property Representation

While plastic analysis-based topology optimization methods exist and can simplify topology optimization—particularly for steel structures—by assuming full plasticity of each member without requiring detailed stiffness matrix computations, these approaches are less straightforward for RC. For example, the GRAND framework developed by [16] efficiently uses plastic collapse mechanisms to directly find optimal steel topologies under ultimate load conditions, bypassing the complexities of elastic compliance minimization. This works well for steel because its behavior closely matches ideal plasticity without complex cracking or tension softening.

However, RC's nonlinear behavior—such as cracking, tension softening, and complex elasto-plastic responses—makes applying full plasticity assumptions at the conceptual stage more challenging and less practical. Therefore, despite the elegance and efficiency of plastic-collapse-based methods for steel, the elastic approach remains preferable for RC topology optimization. It provides a simpler, computationally efficient framework consistent with standard civil engineering practice, where serviceability and load path identification are the main goals.

Both elastic and elasto-plastic analysis frameworks can be incorporated into structural optimization, depending on the design stage and objectives. Linear elastic analysis assumes small deformations and neglects geometric nonlinearity, making it suitable for early-stage conceptual design. It satisfies equilibrium and compatibility conditions and aligns with standard civil engineering practices. In contrast, elasto-plastic analysis captures nonlinear material behavior and ultimate capacity, but is less common in topology optimization due to its computational complexity. Still, it is essential for capturing realistic failure modes and ensuring safety under extreme loading conditions.

In the case of RC building structures, the initial goal is to ensure satisfactory performance under service loads—thus keeping the structure in the elastic range. This justifies the use of an elastic representation of RC during the first stage of ground structure topology optimization, where the objective is to minimize compliance and identify efficient load paths with minimal material use. However, under extreme or ultimate loading conditions, the structure must remain stable and ductile, which requires considering the elasto-plastic behavior of RC materials, including steel yielding and concrete cracking.

4.2. Method Followed

A graph based Latin Hypercube Sampled (LHS) ground structure is first generated. Finite Element Analysis (FEM) is then carried out for these samples to minimize structural compliance. The resulting data are used to train a sparse Gaussian Process (GP) model, and its performance is subsequently evaluated.

 doi:10.20944/preprints202604.0258.v1

For the remaining population—either the unused portion of the LHS sample or a specifically withheld subset—compliance predictions are made using the trained sparse GP model. Ground structures exhibiting minimum compliance, potentially selected from each cluster or category, are identified as optimal candidates.

A subset of these candidates from each category is then selected and subjected to PSO, through which the final optimal configuration is determined.

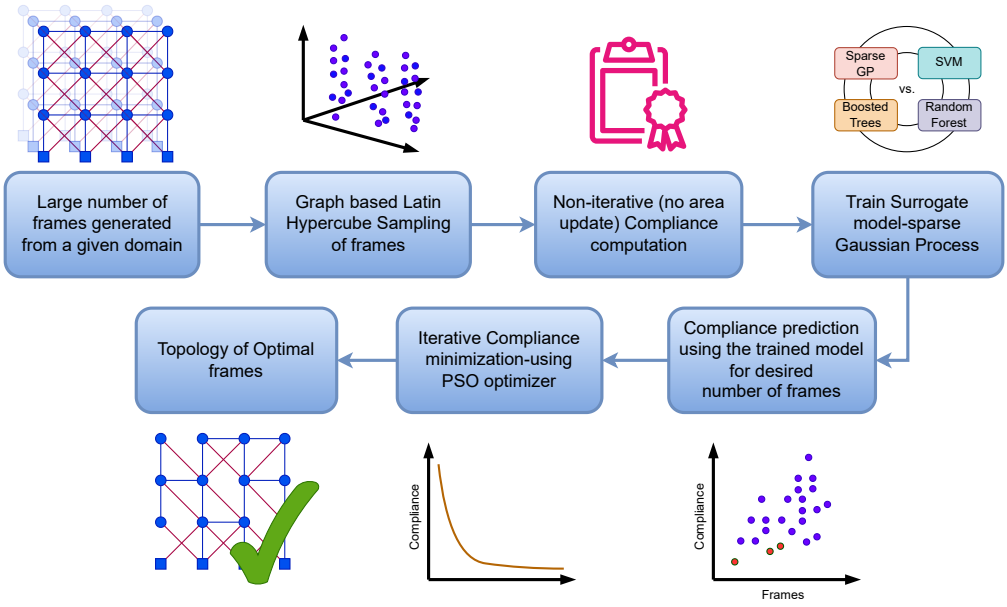

Figure 2. Systematic Pipeline for Topology Optimization of Reinforced Concrete Frames.

5. Compliance Based Optimization

5.1. Objective Function

A compliance minimization problem under volume fraction constraints is mainly defined as

$$\begin{aligned} \min_{a} \quad & C(a) = f^T U(a), \\ \text{s.t.} \quad & K(a)\,U(a) = f, \\ & a_{\min} \le a \le a_{\max}, \\ & \frac{1}{n}\sum_{i=1}^{n} a_i \le V_f. \end{aligned} \tag{10}$$

where:

C	Compliance (objective to minimize),
$f \in \mathbb{R}^m$	External force vector,
$U \in \mathbb{R}^m$	Displacement vector,
$K(a) \in \mathbb{R}^{m\times m}$	Global stiffness matrix (depends on a),
$a = [a_1, a_2, \ldots, a_n]^T \in \mathbb{R}^n$	Vector of design variables (e.g., element densities),
$a_{\min}, a_{\max} \in \mathbb{R}$	Lower and upper bounds on a,
n	Number of finite elements,
$V_f \in (0, 1]$	Prescribed maximum volume fraction.

5.2. Design Variables

The main design variable in the compliance based and stress based optimization is the area. In the computation of stiffness matrix however, the moment of inertia dictates the rigidity. For rectangular

 doi:10.20944/preprints202604.0258.v1

cross sections for example, it is a function of the cross section width and height. Thus, height need to get related to area to avoid multiple variables. The width can then readily be computed from the height.

Accordingly, 324 data point for height and area is generated between height of 0.15m and 1m with 5cm interval for workability. A regression model is then fit to it. Mean and median is taken from the area distribution as shown on the scattered plot.

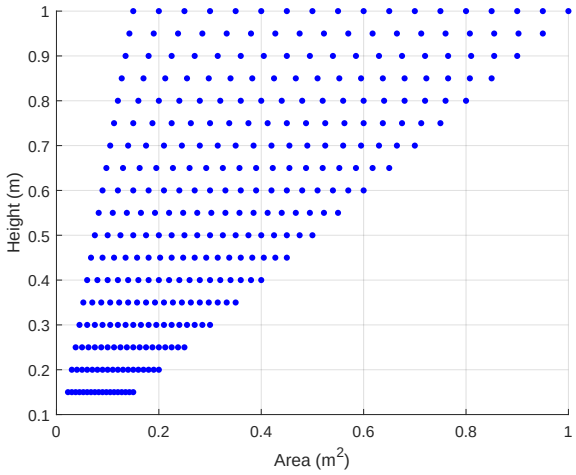

Figure 3. Scatter Plot of Cross-Sectional Area vs. Height for RC Member Sizing Data.

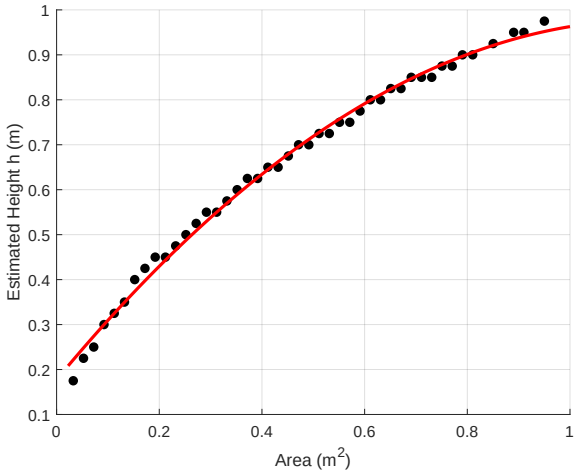

Figure 4. Quadratic Regression Fit of Area Model.

The quadratic regression model fit to predict height is shown on Figure 4.
The estimated regression model for height h in terms of area A is:

$$h = -0.5947\,A^2 + 1.3802\,A + 0.1774. \tag{11}$$

The quadratic regression model has coefficient of determination R^2 value of 0.9951.
Then the moment of inertia I could be approximated from h given area A.

5.3. Constraints and Bounds

Constraints in topology optimization play a crucial role in guiding the algorithm toward practical and safe designs. Fundamental among these are the equilibrium constraints, ensuring that the structure satisfies force and moment balance under the given loading. Volume constraints are commonly imposed to limit total material usage, thereby promoting structural efficiency and sustainability. Additionally, serviceability constraints are important in strength-priority designs, particularly in limiting deflections and vibrations that could impair usability or cause discomfort even when strength

 doi:10.20944/preprints202604.0258.v1

criteria are satisfied. Out of the listed constraints, the volume reduction and area bounds are used for the stage 1 or optimal topology.

- **Volume Reduction:** Limit total volume to a fraction of the original full design:

$$\frac{V_{\text{opt}}}{V_{\text{org}}} - V_f \leq 0. \tag{12}$$

where:
V_{opt} is the volume of the optimized structure, computed as the sum of element volumes using optimal cross-sectional areas,
V_{org} is the volume of the original fully solid design, computed using the maximum cross-sectional area $A_{\max}$ of the optimization input,
V_f is the prescribed volume fraction limit.

- **Cross-Sectional Area Bounds:**

$$A_{\min} - A_e \leq 0 \quad \text{and} \quad A_e - A_{\max} \leq 0. \tag{13}$$

where: A_e is the optimal area of element e, and $A_{\min}, A_{\max}$ are the lower and upper area bounds.

5.4. Penalization

To enforce the satisfaction of physical and design constraints within the optimization framework, a quadratic penalty method is adopted. This method augments the compliance objective function with a penalty term that increases proportionally to the square of the constraint violation. For a given constraint $g_e \leq 0$ on element e, the penalty contribution is defined as:

$$\text{Penalty}_e = \begin{cases} (g_e)^2, & \text{if } g_e > 0, \\ 0, & \text{otherwise.} \end{cases} \tag{14}$$

where: g_e represents the constraint violation measure for element e. expressed by the difference between actual value and its limit.

The total penalized objective becomes:

$$\Pi = \text{Compliance} + \text{penaltyFactor} \times \sum_e \text{Penalty}_e. \tag{15}$$

where: Compliance $= \mathbf{u}^\top \mathbf{F}$ is the structural compliance, and penaltyFactor is a large positive scalar that weights the penalty to strongly discourage violations.

This formulation ensures that the optimizer is steered away from constraint violations while preserving smoothness for gradient-based methods.

5.5. Stopping Criteria

Particle Swarm Optimization (PSO) is selected as the optimizer for compliance minimization in this work due to its demonstrated suitability for RC structural optimization problems. PSO has gained recognition for its simplicity, ease of implementation, and derivative-free nature, making it directly applicable to the non-convex, discrete design space of RC frames without requiring gradient information [17,18].

Convergence is affected by stoppage criteria. The algorithm terminates when either of the following conditions is met:

$$k \geq k_{\max} \quad \text{or} \quad |J^{(k)} - J^{(k-1)}| < \epsilon. \tag{16}$$

where:

 doi:10.20944/preprints202604.0258.v1

k Current iteration number,
$k_{\max}$ Maximum number of allowed iterations,
$J^{(k)}$ Cost function value at iteration k,
ϵ Specified convergence tolerance.

The swarm based PSO optimizer convergence is broadly affected by the population size as well. The larger the population size, the faster the convergence will be. However, it increases the time elapsed.

5.6. Meshing

Mesh size convergence plot is shown. The level of fines can also be taken from the fact that the internal response may not further bring meaningful change in compliance that ultimately leads to change in the size of the design parameters for that element or segment.

Maximum vertical deflection could be computed as:

$$\delta_{\max} = \frac{PL^3}{3EI}. \tag{17}$$

where:

P Point load,
L Length of the beam,
E Modulus of elasticity,
I Moment of inertia.

Similarly, the maximum rotation is given by:

$$\theta_{\max} = \frac{PL^2}{2EI}. \tag{18}$$

Table 1. Maximum Deflection and Rotation vs Mesh Size.

Mesh Size (m)	Max Deflection (μm)	Max Rotation (μrad)
0.5	0.1486	0.5349
0.25	0.3009	0.6687
0.1	0.4044	0.7061
0.05	0.4399	0.7115
0.01	0.4684	0.7132
0.005	0.4719	0.7132
0.001	0.4748	0.7132
Analytical	0.4751	0.7127

A 1m long cantilever beam under 1kN load was discretized between 50 cm and 1mm. The corresponding vertical deflection and rotation were recorded at the tip of the beam. The results were compared with those of the corresponding analytical. The normalized difference between the analytical and the simulated values for deflection reaches 7.4 % at 5cm meshing size, while, for rotation at 10cm meshing size it is only 0.93 %. While 5cm spacing is ideal for detailed values, the compliance is not significantly affected within this range. Hence, considering the computational burden, 10cm meshing size could be fairly adopted. According to the Figure 5, meshing size between 10cm and 25cm could also be considerable ranges for topology optimization especially for preliminary design.

 doi:10.20944/preprints202604.0258.v1

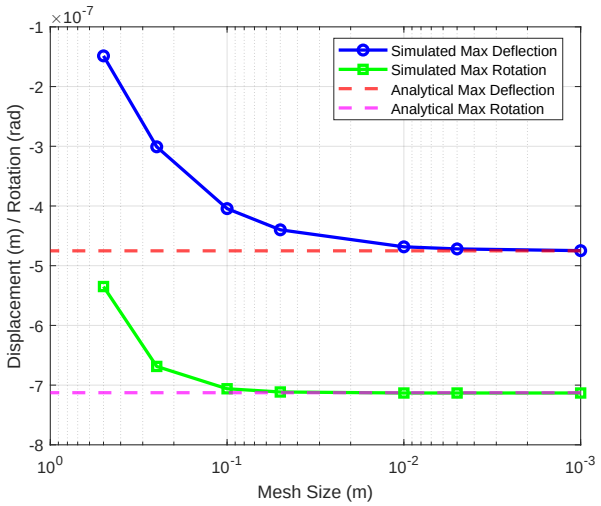

Figure 5. Mesh Size Convergence: Simulated vs. Analytical Maximum Deflection and Rotation for a Cantilever Beam.

5.7. Matrix Singularity Regularizer and Size Threshold

The Frobenius norm $\|\mathbf{K}\|_F$ provides a scalar measure of a matrix's total energy by aggregating the squared magnitudes of all its entries K_{ij}. This norm is particularly useful in structural analysis, where $\mathbf{K} \in \mathbb{R}^{m\times n}$ often represents a global or local stiffness matrix, and each term K_{ij} corresponds to the interaction between degrees of freedom i and j. The threshold τ defines a lower bound below which the matrix or its components may be considered numerically negligible.

$$\|\mathbf{K}\|_F = \sqrt{\sum_{i=1}^{m}\sum_{j=1}^{n} |K_{ij}|^2} \leq \tau. \tag{19}$$

It is used for matrix regularization to ensure invertibility when stiffness matrices become ill-conditioned or nearly singular due to very small values during the numerical solution of equilibrium equations.

$$\mathbf{K}_{\text{reg}} = \mathbf{K} + \epsilon \cdot \|\mathbf{K}\|_F \cdot \mathbf{I}. \tag{20}$$

where:

$\mathbf{K}_{\text{reg}}$	Regularized stiffness matrix,
ϵ	Small regularization factor 10^{-10},
$\mathbf{I}$	Identity matrix of the same dimension as $\mathbf{K}$.

This additive term ensures that $\mathbf{K}_{\text{reg}}$ becomes positive definite and invertible, enabling stable computation of displacements $\mathbf{u}$ from the equilibrium system.

5.8. Element Removal and Area for the Optimal Frame

In post-analysis optimization, ensuring structural efficiency and quality involves two key steps: removing elements with poor mesh quality and assigning a representative area to each retained element. Elements with a high proportion of sub-elements below a minimum area threshold are removed to maintain reliability. For the remaining elements, assigning a uniform area—based on filtered sub-element data—supports consistent structural modeling and fair comparison across the frame. These steps are crucial for achieving both safety and material efficiency in the final optimized design.

To ensure fairness and consistency in selecting the optimal frame after analysis, the quality of meshed elements is evaluated using relative metrics instead of absolute counts. Relying on a fixed number of sub-elements falling below a minimum area threshold $A_{\min}$ can introduce bias, as elements may contain varying numbers of sub-elements. To address this, the removal ratio n_r is

 doi:10.20944/preprints202604.0258.v1

introduced, quantifying the proportion of sub-elements within an element whose areas are less than A_{min}. An element is excluded from further consideration if n_r exceeds a specified threshold, indicating insufficient mesh quality.

$$n_r = \frac{n_{\text{violating}}}{n_{\text{total}}}. \tag{21}$$

where:

$n_{\text{violating}}$	Number of meshed sub-elements within the parent element area less than A_{min},
n_{total}	Total number of meshed sub-elements within the element,
n_r	Removal ratio.

In an effort to assign a uniform area to each element, while assigning the maximum area guarantees safety by accounting for the worst-case requirement, it may lead to overly conservative and uneconomical designs. A more balanced and cost-effective approach involves using the mean area of valid meshed sub-elements—those not filtered out by the removal ratio criterion. This supports both structural performance and material efficiency. In this work, the mean is preferred, and the representative area for each element is computed as:

$$A_{\text{elem}} = \frac{1}{n} \sum_{i=1}^{n} A_i. \tag{22}$$

where:

A_{elem}	Assigned uniform area of the element,
A_i	Area of the i-th meshed sub-element that satisfies the minimum area condition,
n	Number of such valid sub-elements used in the averaging process.

It is important to note that in structural systems such as building frames designed to support slabs, beam elements are typically subjected to distributed gravity loads, and due to their structural function, they may be exempted from the element removal criteria. These frames prioritize continuity and vertical load transfer, making removal of elements potentially unrealistic.

5.9. Optimal Frame Validation

This process ensures that elements contributing minimally to stiffness often artifacts of numerical regularization or penalization are excluded, leading to a cleaner and more manufacturable design. The compliance of the pruned frame is then recomputed under the same external loading conditions as used during the optimization phase. This step validates whether the structure maintains acceptable stiffness after element removal and helps assess the structural integrity of the simplified design.

The validation process involves comparing two key performance indicators: the increase in structural volume and the change in compliance. A volume increase beyond a certain threshold may indicate excessive compensation for stiffness loss through remaining elements, undermining the material-efficiency goal. Simultaneously, a significant increase in compliance suggests a detrimental impact on structural stiffness. Such metrics are compared against their respective tolerances to determine if the final design remains within acceptable bounds. This evaluation ensures that the trade-off between weight savings and structural performance is well-balanced and that the design meets both mechanical and optimization objectives.

$$C_{\text{norm}} = \frac{C}{\|F\|^2}. \tag{23}$$

where:

C	Original compliance before optimization,
$\|F\|^2$	Squared norm of the original load vector,
C_{norm}	Normalized original compliance.

 doi:10.20944/preprints202604.0258.v1

$$C_{\text{opt, norm}} = \frac{C_{\text{opt}}}{\|F_{\text{filtered}}\|^2}. \tag{24}$$

where:

C_{opt}	Compliance after reanalysis of the filtered optimized frame,
$\|F_{\text{filtered}}\|^2$	Squared norm of the filtered load vector,
$C_{\text{opt, norm}}$	Normalized optimized compliance.

Post-optimization reanalysis naturally increases compliance as element removal leads to stiffness loss, a well-documented phenomenon in structural topology optimization (both density- and ground-structure-based). In practice, pruning very low-density or low-area members typically causes a modest rise in compliance on the order of 5–15%, while larger increases (above about 20%) are generally taken to indicate that the pruning has significantly altered the optimal load paths, as reported in recent post-editing and robustness studies for topology-optimized lattices and continua [19–21].

For reinforced concrete frames specifically, a 20% C_v tolerance is reasonable because members are physically bounded by constructability requirements such as aggregate flow and rebar clearance, which preclude the infinitesimal member sizes often allowed in steel topology optimization. In addition, the mandatory retention of floor beams to ensure slab support introduces small compliance penalties that are secondary to detailing feasibility and structural continuity [22]. Within this framework, a $C_v \leq 5\%$ threshold identifies very conservative layouts that retain near-original stiffness, while $C_v \leq 20\%$ marks high-efficiency solutions that remain compatible with practical RC detailing and frame behavior [23].

$$C_v = \frac{C_{\text{opt, norm}} - C_{\text{norm}}}{C_{\text{norm}}}. \tag{25}$$

where:

C_{norm}	Normalized original compliance,
$C_{\text{opt, norm}}$	Normalized optimized compliance,
C_v	Compliance validation metric (relative change).

6. Surrogate Model for Compliance Prediction

6.1. Latin Hypercube Sampling

LHS was used to efficiently select a representative subset of frame structures from a large design space, ensuring broad coverage of the input domain with reduced computational cost [24]. Parameters included both geometric and topological attributes relevant to frame design, such as nodal coordinates, member connectivity, number of stories and bays, bay width, and story height. Higher-level features like inclined columns, connectivity level, and structural cluster membership were also considered. Each parameter range was divided into equal intervals, with one value sampled per interval and sampling orders permuted to avoid inter-variable correlation. The full parameter set is:

$$\begin{aligned} P = \{&\text{Bay Width}, \text{ Story Height}, \text{ Number of Bays}, \\ &\text{Number of Stories}, \text{ Nodes Matrix}, \text{ Connectivity Matrix}\}. \end{aligned} \tag{26}$$

Original ground structures and their perturbed variants were both included, ensuring diversity and representativeness across categories.

Graph Approach

An alternative to vectorizing raw nodal coordinates is to represent each structure as a graph, enabling feature extraction aligned with graph neural network (GNN) applications. This approach captures both topological and geometric properties using a compact set of descriptors [25,26]. Key features include the number of nodes and edges (numN, numE), average and maximum node degrees (mean(deg), max(deg)), and graph diameter (max(D)). Structural flow is characterized by average

 doi:10.20944/preprints202604.0258.v1

betweenness centrality (mean(bc)), while geometric variation is captured through mean and standard deviation of edge lengths. The spatial footprint is approximated by the product of coordinate ranges, and overall connectivity is quantified by graph density $\left(\frac{2\cdot\text{numE}}{\text{numN}(\text{numN}-1)}\right)$. The resulting feature vector is:

$$\begin{aligned} F = \{&\text{Number of Nodes, Number of Edges, Average Degree, Maximum Degree,} \\ &\text{Graph Diameter, Average Betweenness Centrality, Mean Edge Length,} \\ &\text{Edge Length Std. Dev., Bounding Box Volume, Graph Density}\}. \end{aligned} \tag{27}$$

Once F is returned from P, LHS is applied to F for a desired number of iteration. Moreover, since graph-based features form a fixed-length vector regardless of the varying size and connectivity of each frame, LHS can be applied uniformly across all generated frame configurations, ensuring diverse and representative coverage of the design space.

6.2. Gaussian Process Surrogate Model

In this study, a sparse GP surrogate is trained to predict the compliance of a given ground structure based on a set of frames with computed compliance. A Radial Basis Function (RBF) kernel is chosen for the GP due to its smooth response to changes in input parameters.

The surrogate model predicts compliance directly, bypassing the need for nodal displacement and FEM-based compliance calculations.

A sparse GP approximation, in which only $m \ll n$ representative inducing points are used, reduces the computational complexity from $\mathcal{O}(n^3)$ for a full GP to $\mathcal{O}(nm^2)$, making it tractable for the large frame populations considered in this work.

6.2.1. Sparse Gaussian Process Definition

The sparse GP is defined as:

$$f(x) \sim \mathcal{GP}\big(m(x), \tilde{k}(x, x')\big). \tag{28}$$

where:

$m(x) = \mathbb{E}[f(x)]$	Mean function, expected value of the function at input x,
$\tilde{k}(x, x')$	Approximate covariance function defined using inducing points.

The approximate kernel $\tilde{k}(x, x')$ is computed as:

$$\tilde{k}(x, x') = k_{xZ} K_{ZZ}^{-1} k_{Zx'}. \tag{29}$$

where:

k_{xZ}	Covariance vector between input x and the inducing points Z,
K_{ZZ}	Covariance matrix between the inducing points,
$k_{Zx'}$	Covariance vector between inducing points and input x'.

6.2.2. Radial Basis Function Kernel

The RBF kernel used to define the covariance terms is given by:

$$k(x, x') = \sigma^2 \exp\left(-\frac{\|x - x'\|^2}{2l^2}\right). \tag{30}$$

where:

σ^2	Variance parameter (scale of the kernel),
l	Length-scale parameter, controlling the smoothness,
$\|x - x'\|^2$	Squared Euclidean distance between input vectors x and x'.

 doi:10.20944/preprints202604.0258.v1

7. Case Study: Optimal Ground Structure Based Reinforced Concrete Frame Optimization

In this section, building domain of width to height aspect ratio of 1:1 and 1:1.5 are examined under gravity loading. The candidate frames could vary in both the number of stories and bay, in addition to the width and height of the bay. Hence, the number of top nodes could also vary for the sake of fairness, the same amount of gravity loading is shared among the top nodes of each frame at the non-iterative compliance computation and prediction stage. Volume constraints are considered for the optimization. Materials C30/37 and S400 based on [27] with elasticity and reinforcement ratio of Ec 33GPa, Es 200GPa are used. The detailed procedure set in the above section is followed throughout the ground structure-based topology optimization of RC frames.

Gravity loads are applied as equal downward nodal forces distributed among all non-base nodes to simulate floor-level loading at every story, and a notional lateral load is applied at the topmost left node to account for geometric imperfection effects per [27]. All base nodes are fully fixed, restraining translational and rotational degrees of freedom.

The PSO optimizer is used in the final stage of this pipeline: that is, in the size optimization of systematically selected candidate topologically optimal frames. The PSO parameters are kept the same across all considered frames.

Table 2. PSO Parameters and Values used.

Parameter	Value
Population size	10
Maximum iteration	100
Inertia weight	0.5
Cognitive coefficient	1.5
Social coefficient	1.5

7.1. Implementation Verification

The FEM implementation is developed in MATLAB (version 2023), and verification of the computational script is essential to ensure its accuracy and reliability. For this purpose, a one-bay, two-story frame consisting of six elements was modeled and analyzed using both the MATLAB code and a commercial FEM software, ANSYS(version 2023 R1). Models of the same frame were created, meshed, and subjected to various loading conditions including lateral point loads, distributed gravity loads, and gravity point loads. The cross-sectional properties, mesh sizes, applied loads, and resulting internal responses such as stresses and displacements were recorded. A comparative analysis of the stresses and deflections obtained from MATLAB and ANSYS was performed to evaluate similarities and differences between the two solutions.

It is important to note that the primary objective of the MATLAB script is to accurately predict displacements, particularly lateral deflections. While stress results from MATLAB and ANSYS are compared, some discrepancies are expected due to differences in modeling assumptions and the level of detail considered by the two FEM approaches. For example, the MATLAB script may not include all the structural components or effects taken into account by ANSYS. Despite these differences, close agreement in displacement results verifies the effectiveness of the MATLAB implementation for its intended purpose.

 doi:10.20944/preprints202604.0258.v1

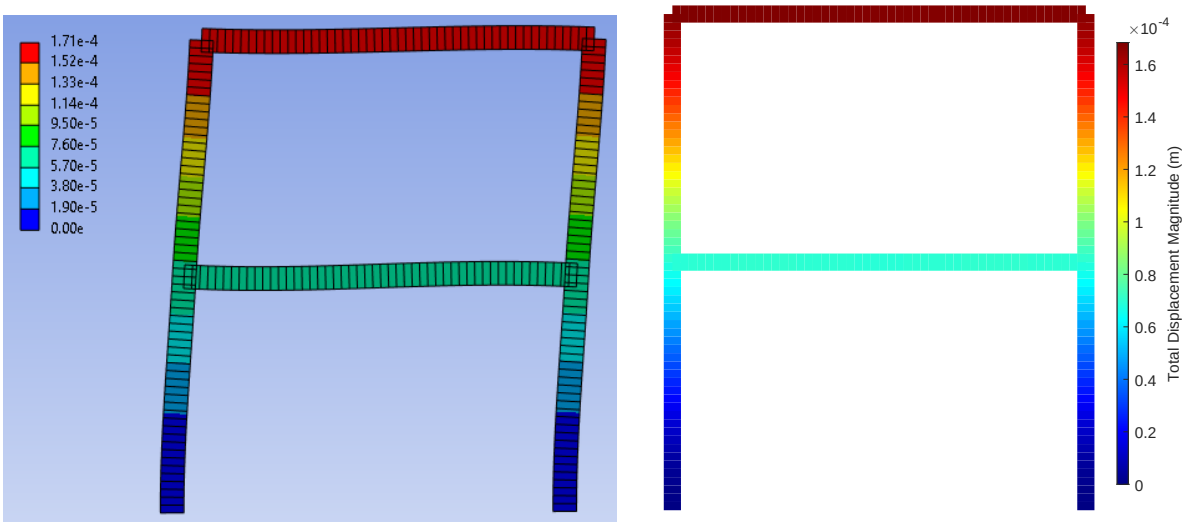

(a) ANSYS Verification **(b)** MATLAB Verification

Figure 6. 2D Frame Verification.

A 1 kN point load is applied horizontally to the right at the top left node. A square cross section with a side length of 30 cm is used. According to MATLAB, the maximum total deformation is 1.68×10-4, which closely matches the result obtained from ANSYS which is 1.71e-4.

7.2. Effect of Nodal Location Interval

To investigate the effect of nodal location intervals, different combinations of spacing along the x- and y-axes were tested: $(0.2, 0.2)$, $(0.2, 0.5)$, and $(0.5, 0.2)$. A domain with aspect ratio of 1:1 which is presented in the subsection below is considered.

The first pair $(0.2, 0.2)$ results in a significantly large number of computational frames, making it computationally expensive. Due to the small interval, a slightly larger spacing may be more efficient.

The second and third combinations, $(0.2, 0.5)$ and $(0.5, 0.2)$, yield a comparatively similar number of frames, both of which are more manageable.

For each of the three interval configurations, a graph-based LHS scattered plot was generated to visualize the distribution of nodal locations.

The clusters are almost similar across the plots. The PC3 axis of Figure 7c reduced to 0.5 could be taken as a small reduction in identification of the samples. Hence, Figure 7b could be chosen in this case.

The second and third nodal location intervals were compared: the second produced 446 unique samples with sampling 2%, resulting in RMSE = 2.0696, MAE = 1.2473, and R^2 = 0.9842; The third yielded 409 unique samples with the same sampling rate 2%, achieving RMSE = 1.8961, MAE = 1.1727, and R^2 = 0.9887. While the third one shows slightly better model performance, the second benefits from a relatively greater number of samples. For a 1:1 domain, both approaches could be considered equivalent. However, the second one is selected to take advantage of the larger dataset for potentially better generalization. Results for different aspect ratio may vary from what is found here.

 doi:10.20944/preprints202604.0258.v1

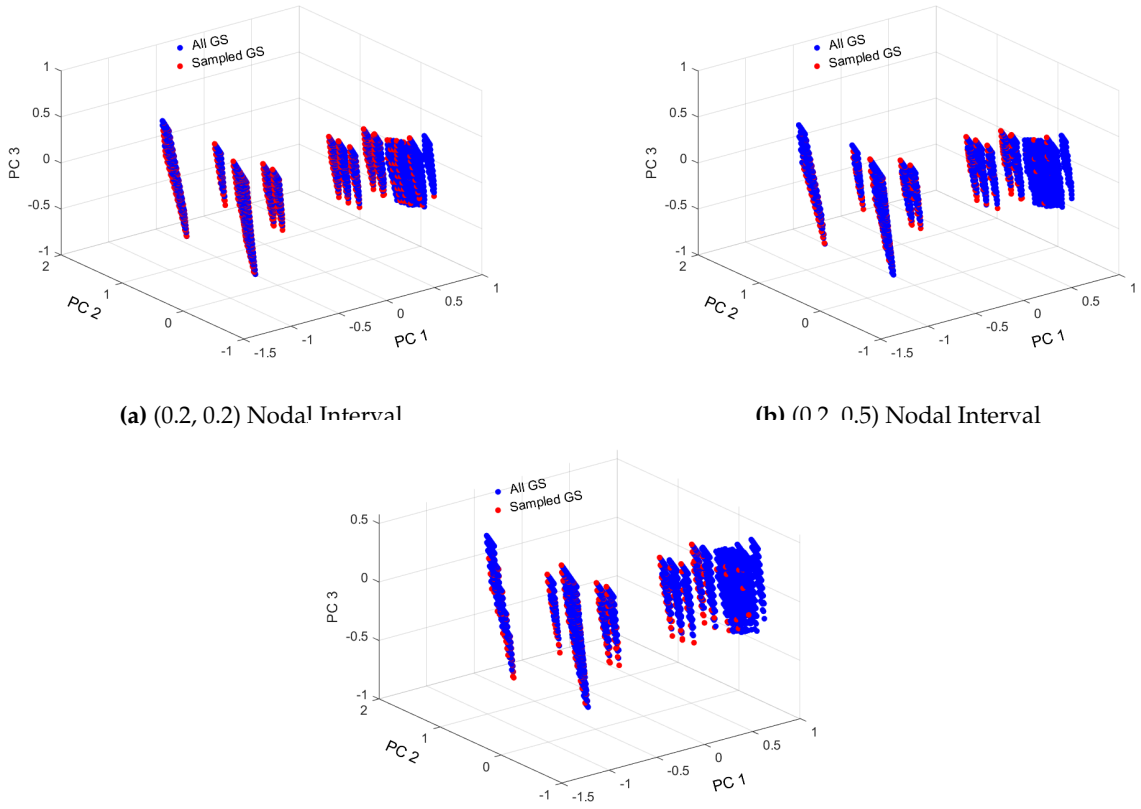

(a) (0.2, 0.2) Nodal Interval

(b) (0.2, 0.5) Nodal Interval

(c) (0.5, 0.2) Nodal Interval

Figure 7. Scattered Plot of Graph based LHS sampled with Different Nodal Intervals for a 1:1 Aspect Ratio Domain.

7.3. Performance of Multiple Models

Apart from sparse GP, support vector machine(SVM), random forest(RF) and gradient boost(GB) models were used and compared. In multiple cases, the sparse GP could preferable. For the $(0.2, 0.5)$ nodal interval range discussed above, the performance of these models is summarized on Figure 8.

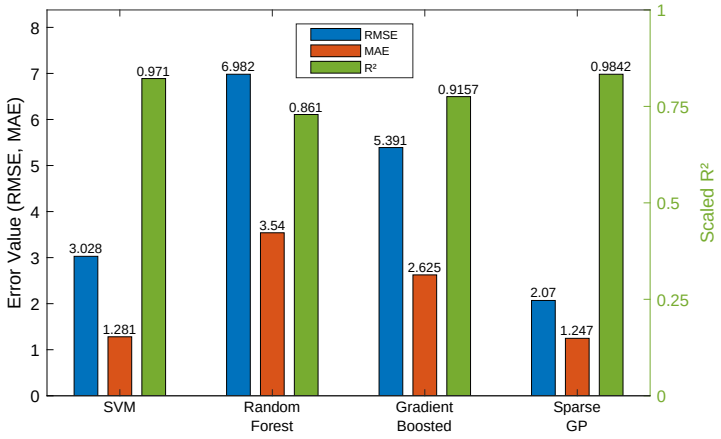

Figure 8. Model Comparison for Compliance Prediction.

7.4. Frame with 1:1 Aspect Ratio

Width of 10m and height of 10m domain is used. Bay width bound of $[3m, 7m]$ and story height bound of $[2.8m, 4m]$ are set. Nodal location is allowed to be generated with interval of 0.2 m along both axes. This generated 26208 basic ground structures and a total of 438984 ground structures when perturbation is considered. Though the level of connectivity could differ, for any of those level 1, level 2 or fully connected level the total number of GS remains the same. Perturbation of 0.2m is

 doi:10.20944/preprints202604.0258.v1

used. Though Level 1 and fully connected levels were considered, the optimization mainly focused on the level 2 connectivity where each node is allowed to get connected to its next node beyond the immediate neighbor node. This could be taken as an intermediate connectivity between level one and fully connected connectivities there by excluding potentially slender elements. The computational load is further reduced by increasing the nodal location interval along the elevation to 0.5m. Accordingly, the total number of GS reduces to 63784.

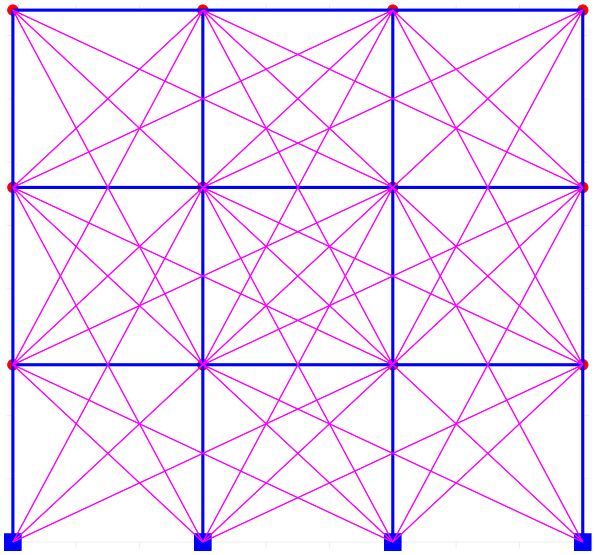

Figure 9. Typical Frame with Aspect Ratio of 1:1 and Level 2 Connectivity.

7.4.1. Graph Based LHS Sampling

The graph based LHS considers important features that could dictate load flow along the frames. This method usually returns multiple same frames to be important or strong neighbors. Hence, the graph based LHS approach needs to get filtered once sampling is done to return unique frames. Or one may consider those repeated frames and their frequency as the importance indicator of those frames to be included as samples or even directly as final candidate frames that might be considered for the intended actual topology optimization at the end of this procedure.

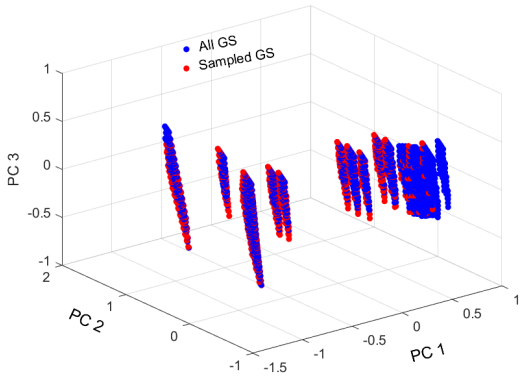

Figure 10. PCA Scattered Plot for Graph-based LHS of Frames.

 doi:10.20944/preprints202604.0258.v1

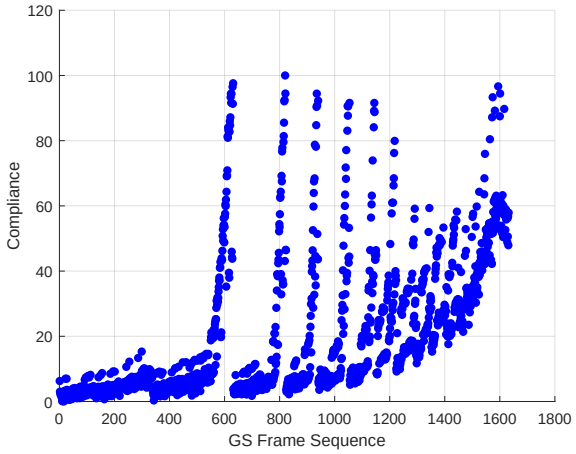

Figure 11. Compliance of Sampled Frames under same material volume (normalized and scaled to 100).

Although the number of samples depends on the number of variables or features, a sampling of consistently 20 % is used. 1632 unique LHS samples returned. Figure 10 shows how the sampled frames are representative to the population after reducing the dimensionity of the principal component analysis (PCA). The clusters are usually influenced by the number of bays, number of stories and their widths and heights. And the layers within each cluster represent frames varied with bay width and story height.

7.4.2. Sparse Gaussian Process Based Compliance Prediction and Candidate Frame Selection

The next step is to compute the compliance of these sampled frames. An elastic analysis of the RC frame with an equivalent material property is used. Meshing size of 0.2 is also consistently used. Each frame is loaded with 10kN point load at its top nodes being shared to the available number of top nodes. For each frame, uniform area of elements is used. However, to maintain the same volume of material for each frame, the area of each frame is computed by equating to the volume of the first frame. The area for the first frame could be reasonably given by:

$$A_{f_{i+1}} = \frac{V_{f_1}}{L_{f_{i+1}}}, \quad i = 1, \ldots, n-1. \tag{31}$$

where:

$A_{f_{i+1}}$ is the area of frame $i+1$,
V_{f_1} is the volume of frame 1,
$L_{f_{i+1}}$ is the total length of the elements of the frame $i+1$,
n is the number of samples.

Therefore, this compliance does not involve any iteration, optimization, or penalization. Its main objective is to roughly estimate the compliance or stiffness of each frame given relatively the same scenario. The computed values are scaled to 100 for common visualization.

The trend in the Figure 11 plot seems to correspond to the clusters and layers of the scattered LHS plot here in Figure 10. Those frames with smaller compliance are those with relatively smaller bay width and story height. Though it is difficult to generalize, frames with more number of bays and stories as well have smaller compliance. Larger compliances correspond to fewer bays and more stories.

 doi:10.20944/preprints202604.0258.v1

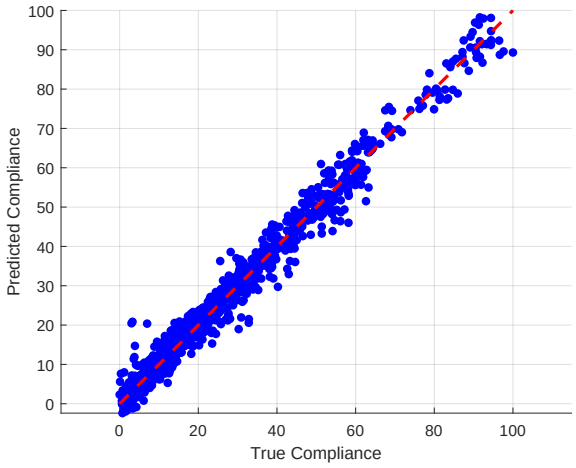

Figure 12. Sparse Gaussian Process Model for frames with 1:1 Aspect Ratio Domain (normalized and scaled to 100).

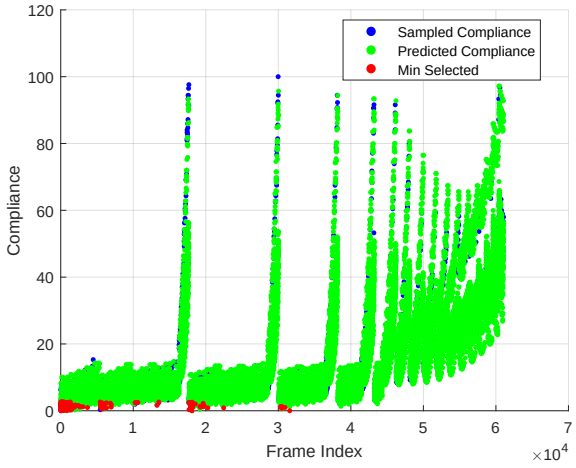

Figure 13. Compliance Prediction Map of Frames based on the Trained Model for 1:1 Aspect Ratio Frame Domain.

80:20 % data split is used to train the sparse Gaussian Process model. And a K fold cross validation with K=5 is implemented. The performance of the model returned less RMSE and MAE with values of 2.5706, 1.7481 respectively. The coefficient of determination R^2 0.9847 is also quite convincing.

The final step to identify potential frame/s for topology optimization out of large domain of potential frames is making prediction of the compliance of the rest frames using the trained model.

Therefore, prediction is made to the rest 59432 frames. For the sake of visualization, 200 candidate frames are highlighted, in which 100 from those used to train the model and 100 from those predicted, based on their minimal compliance score.

From Figure 13 it is observable that the prediction is fitting to the existing computed samples. All the frames within the first cluster, up to around 15000 frames have the maximum number of bays, number of story within the given domain and interval width. A frame with more number of bays and having relatively larger story height also returns smaller compliance (frames 3309 and 9881).

Frames within the same cluster are affected by their height in the story and the width of the bay. Frame 3 for example has less compliance than Frame 111 because the latter has a relatively larger story height at its second story. Hence, those frames with maximum number of bays and maximum number of stories, being other criteria considered here kept same, are preferably returning lowest compliance, hence could be chosen for compliance minimization as potential ground structures.

The advantage of this graph-based LHS and GP-guided selection over naive random candidate selection is twofold. First, graph-based LHS ensures structural diversity across the sampled frames covering variations in bay count, story count, connectivity level, and geometric perturbation rather

 doi:10.20944/preprints202604.0258.v1

than clustering around geometrically similar configurations as random sampling would. Second, the trained GP model ranks all remaining frames by predicted compliance, enabling targeted identification of low-compliance candidates across the full frame population without exhaustive FEM evaluation. As demonstrated in Figure 13, this combined mechanism ensures that candidates forwarded to PSO are both structurally representative and compliance-efficient, significantly reducing the computational cost of downstream topology optimization.

7.4.3. Compliance Minimization of Selected Candidate Frames Using PSO Optimizer

Now, iteration-based topology optimization can be applied to any desired number of frames with smaller compliance according to Figure 13. Or if there is a strong desire to specific number of bays or stories or bay width and story height or their combinations, frames could be selected from appropriate cluster or region from the candidate GS Selection map shown on Figure 13.

The final step could either be computed by considering only volume constraint to attest the appropriateness of those selected frames as candidate ground structures or constraints that map the real-world scenario could be considered.

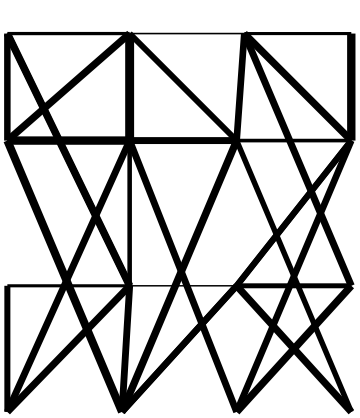

(a) Optimal Frame

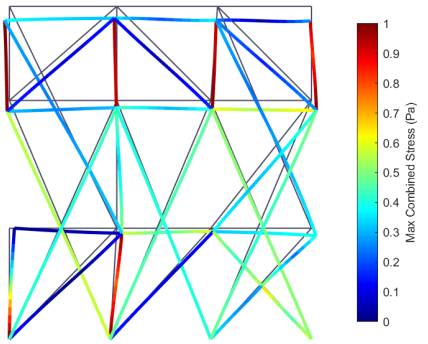

(b) Deformed Shape (scaled up 1000 times) and Stress Distribution

Figure 14. Optimal Frame with Index 19634.

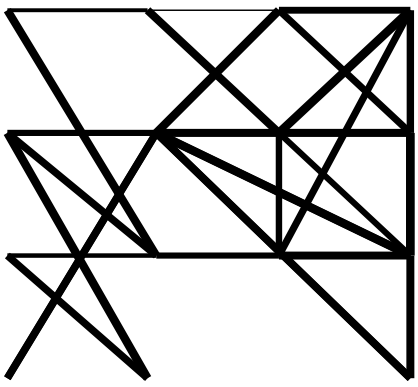

(a) Optimal Frame

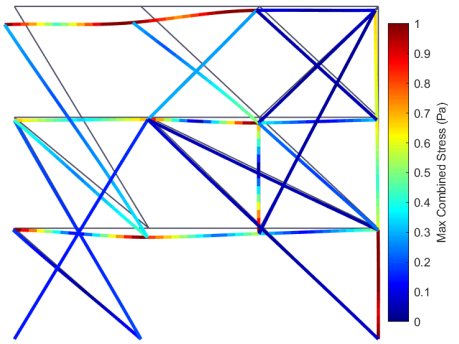

(b) Deformed Shape (scaled up 1000 times) and Stress Distribution

Figure 15. Optimal Frame with Index 18237.

Table 3. Summary of Optimal Frame Parameters.

Frame index	No. elem	Opt elem	V_f	n_r	C_v	norm A_{min}
19634	81	35	0.544	0.15	0.144	0.455
3	95	40	0.518	0.18	0.12	0.506
18273	93	26	0.53	0.17	0.16	0.328

 doi:10.20944/preprints202604.0258.v1

The verification procedure for frame index 19634 as shown in Figure 14 reserved only 45.6 % ($1 - V_f$) of the initial elements domain. The increase in compliance after element removal is limited to 14.4 % only. As the frame is mainly for building purpose, thinner beams are kept from removal. The minimum area accounts for 0.455 of the normalized area scale, indicating that a considerable number of elements are retained at the minimum allowable area. This is attributed to the exclusion of floor beams from the element removal criterion, as their continuity is necessary to ensure practical slab support at every story level based on the assumption considered in this work. It is worth noting that without this floor beam retention requirement, the optimal frames would consist of significantly fewer elements, yielding sparser and more material-efficient topologies. The deflected shape is scaled up by 1000 times. According to Figure 14b, top columns are under high stress while the immediate lower columns, being multiple elements share the stress, are relatively less stressed.

The optimal frame Figure 15a mainly relayed more on diagonal elements than the vertical columns. The pattern of their arrangement also contributed to larger space formation.

Table 4. Volume Fraction Comparison in Topology Optimization Literature.

Structure Type	Vf Range	Vf Definition	Ground Structure	Notes
Steel trusses [28]	0.10–0.25	$V_{\text{opt}}/V_{\text{domain}}$	Dense/fully connected	Unrealistic for RC
Steel frames [23]	0.35–0.50	$V_{\text{opt}}/V_{\text{allowed}}$	Dense GS	Stress-based
RC beams [22]	0.40–0.60	$V_{\text{opt}}/V_{\text{concrete}}$	Truss-continuum	ASCE benchmark
RC frames [this work]	0.5–0.6	$V_{\text{opt}}/(\sum A_{\text{i,max}} L_i)$	Sparse/systematic	addressed constraints

The volume fractions of $0.5 - 0.55$ (Tables 3 and 5) demonstrate RC frame efficiency, surpassing benchmarks in Table 4 despite constructability constraints (min. rebar/aggregate dims).

The systematic GS generation, realistic bay widths ($3 - 7$m), story heights ($2.8 - 4$m), limited connectivity (Level 1/2) and nodal perturbation ($\delta = 0.2$m) yields sparse, practical topologies. Unlike dense steel truss/frame topology optimization's single fully connected GS (enabling unrealistically low Vf via thin, non-buildable members), this balances compliance minimization under gravity loads with RC feasibility.

7.5. Frame with 1:1.5 Aspect Ratio

Tall frames could be represented by this case. The procedure is once again the same. Total of 104032 GS are generated from 1870 basic GS with node location interval 0.5, 0.5.

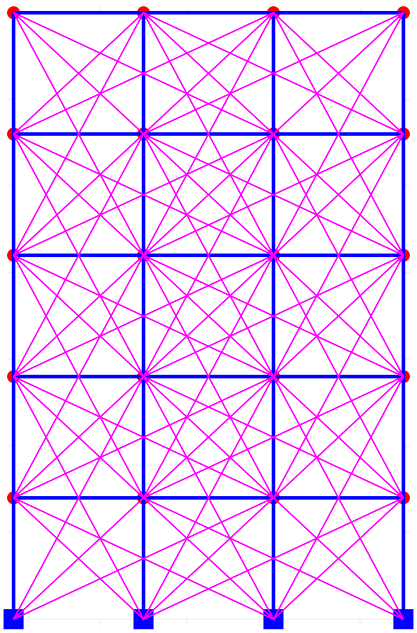

Figure 16. Typical Frame with Aspect Ratio of 1:1.5 and Level 2 Connectivity.

 doi:10.20944/preprints202604.0258.v1

After 2 % sampling for the sake of computational burden, 615 unique samples are returned.

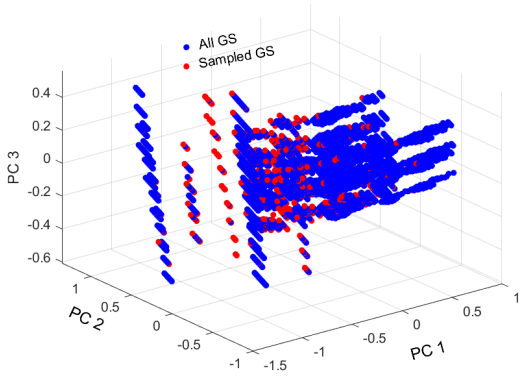

Figure 17. Scattered Plot for PCA reduced Graph-based LHS Samples of Frames.

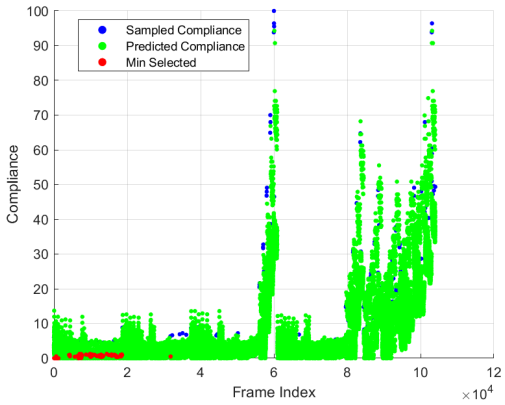

Figure 18. Compliance Prediction Map of Frames based on the Trained Model.

A sparse Gaussian Process model is trained using the computed compliance of these samples. It has $RMSE$, MAE and R^2 values of 3.6094, 1.8605 and 0.939 respectively.

103417 frames received their compliance prediction using the trained model. And desired number of frames are sampled based on their compliance value.

Table 5. Summary of Optimal Frame Parameters.

Frame index	No. elem	Opt elem	V_f	n_r	C_v	norm A_{min}
17446	104	47	0.544	0.23	0.09	0.502
75	131	46	0.549	0.21	0.13	0.3

It can be observed that the optimal frames still consist of more elements than would be expected in a similar structure made of steel. This could be primarily due to two factors. First, the compressive strength of RC is significantly lower than that of structural steel, especially under gravity loading as in the current case. This reduction in compressive capacity has a substantial impact on the structural response, requiring more load-bearing elements in RC designs. Second, since the frames are intended for building applications, beam elements with even smaller area are preserved from removal. This constraint leads to an increased number of elements and forces the optimizer to follow less efficient load paths.

 doi:10.20944/preprints202604.0258.v1

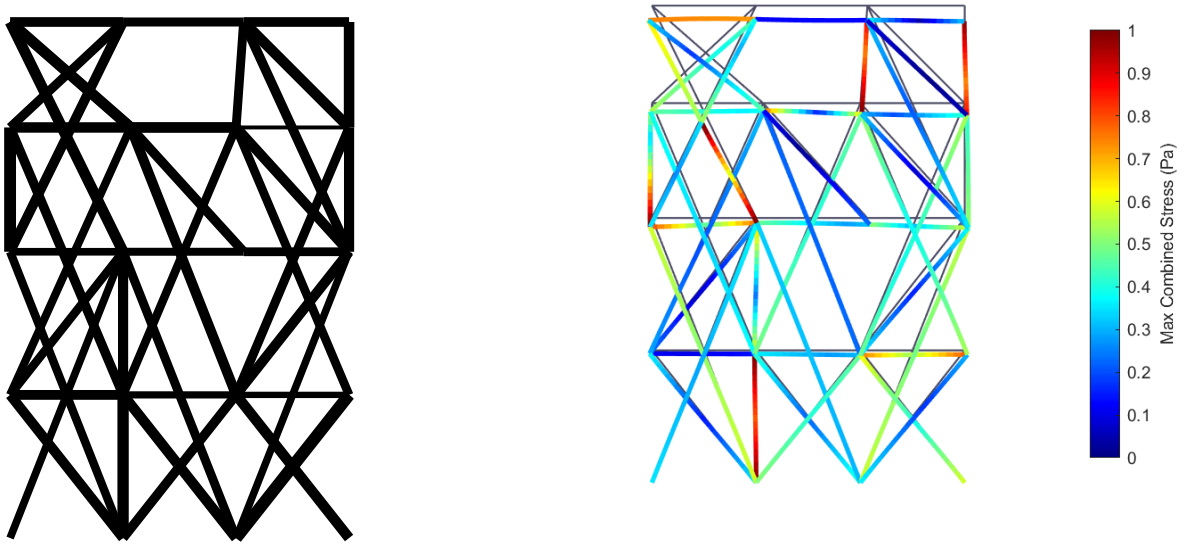

(a) Optimal Frame **(b)** Deformed Shape (scaled up 1000 times) and Stress Distribution

Figure 19. Optimal Frame with Index 17446.

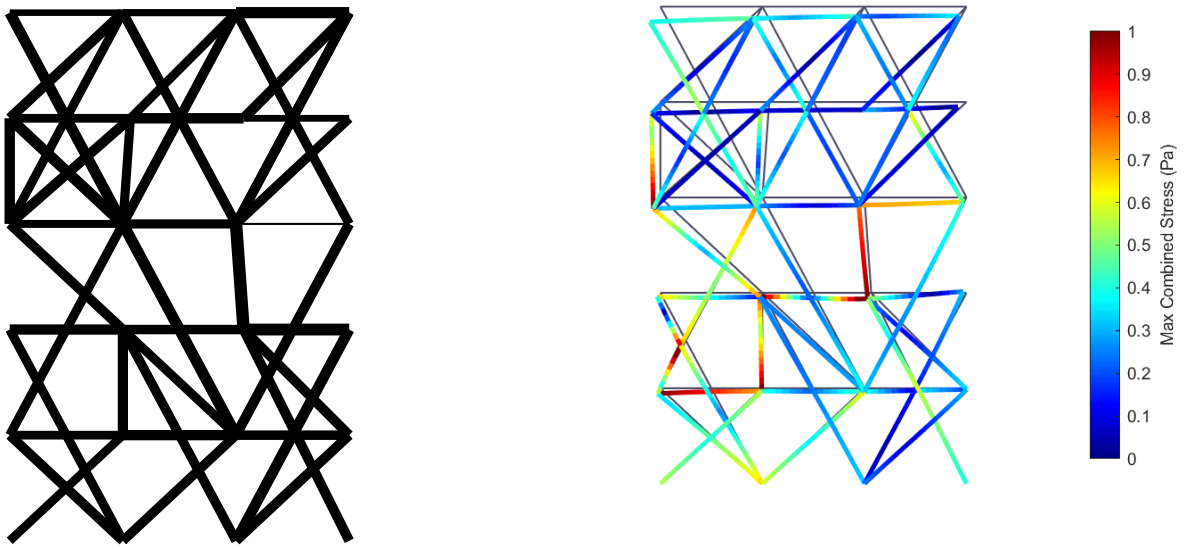

(a) Optimal Frame **(b)** Deformed Shape (scaled up 1000 times) and Stress Distribution

Figure 20. Optimal Frame with Index 75.

The contribution of diagonal elements largely replaced the need for floor columns in most of the stories. As expected for an optimal load path, it is rare to see diagonal elements becoming discontinuous immediately below their lower connected nodes. Such discontinuities result in load being transferred to the beams, which are primarily designed to resist bending rather than axial loads like columns. An example of this can be seen at the second story, third bay node in Figure 20b. This discontinuity correlates with an observable increase in floor deformation in that region.

Conclusion

This work contributes a novel framework for the topology optimization of reinforced concrete building frames, addressing the unique structural characteristics of RC systems, such as sparse connectivity and rigid orthogonal joints. By developing a graph-based ground structure generation method combined with Latin hypercube sampling and surrogate modeling, the proposed approach

 doi:10.20944/preprints202604.0258.v1

enables efficient exploration of a vast configuration space without relying on full-scale iterative optimization for every candidate.

The use of a sparse Gaussian Process model to predict compliance values across unsampled frame configurations proved effective in identifying structurally promising ground structures. These were subsequently refined through compliance minimization using Particle Swarm Optimization, yielding optimal frame designs for two representative domains with distinct aspect ratios.

The case study demonstrated that the optimal load transfer path for frames subjected to gravity loads at the top nodes involved an integrated system of vertical and diagonal elements, which led to the removal of vertical elements such as columns on the intermediate and lower floors.

Importantly, the integration of story beams exempt from the element removal rule allowed for the retention of essential structural integrity while achieving volume fractions below 0.55 in all optimized cases. A notable proportion of elements converge to the lower area bound, a direct consequence of enforcing floor beam continuity for slab support. Relaxing this requirement would naturally lead to considerably sparser structural configurations with a reduced element count. This demonstrates that the proposed approach holds significant potential for generating efficient and RC frame designs. The presented methodology offers a scalable and data-informed path forward for early-stage structural exploration and optimization in RC building design.

The candidate GS selection map, which illustrates considered frames alongside their predicted compliance at an early stage, not only avoids nonstrategic or non-systemic use of GS but also streamlines the selection process. This significantly reduces the computational cost and time required for downstream tasks. Moreover, the map serves as a key reference for understanding the influence of frame parameters and enables candidate GS selection based on specific sub-parameters, such as the desired number of bays and stories required for the structure.

This study has several limitations. The analysis is restricted to two-dimensional RC frame models and assumes linear elastic material behavior, which does not capture nonlinear cracking or yielding effects. Gravity loads and idealized lateral loads are considered, while other load combinations and seismic effects are not explicitly treated. Nonetheless, using linear elastic analyses for candidate ground structure selection is a reasonable choice at this conceptual stage, as it enables efficient screening of large design spaces before more detailed nonlinear assessments. Nonlinear and fully three-dimensional extensions of the proposed pipeline are being developed in separate ongoing studies and will be reported in future work.

Author Contributions: Conceptualisation, Y.L.A.; methodology, Y.L.A.; resources, Y.L.A, B.H., G.U., C.W. and T.L.; software, Y.L.A.; validation, Y.L.A.; writing—original draft preparation, Y.L.A.; writing—review and editing, Y.L.A, B.H., G.U., C.W. and T.L.; supervision, Y.L.A., B.H., G.U., C.W. and T.L. All authors have read and agreed to the published version of the manuscript.

Funding: This work was supported by a special fund of the German government at the BMBF [grant number: 16DKWN078A].

 doi:10.20944/preprints202604.0258.v1

Institutional Review Board Statement: Not applicable.

Informed Consent Statement: Not applicable.

Data Availability Statement: The data presented in this study are available within the article.

Acknowledgments: This work was supported by a special BMBF fund for the Intelligente Methoden zur automatischen und nachvollziehbaren Analyze umfangreicher Infrastruktur-, Verkehrs- und Umweltmessdaten (InMeA) project [grant number: 16DKWN078A]. The BMBF is therefore acknowledged for the funding provided.

Conflicts of Interest: The authors declare no conflict of interest. The funders had no role in the design of the study; in the collection, analyses, or interpretation of data; in the writing of the manuscript; or in the decision to publish the results.

References

1. Changizi, N.; Jalalpour, M. Topology optimization of steel frame structures with constraints on overall and individual member instabilities. *Finite Elements in Analysis and Design* **2018**, *141*, 119–134.
2. Zhang, X.; Maheshwari, S.; Ramos Jr, A.S.; Paulino, G.H. Macroelement and macropatch approaches to structural topology optimization using the ground structure method. *Journal of Structural Engineering* **2016**, *142*, 04016090.
3. Han, Y.; Lu, W.F. A novel design method for nonuniform lattice structures based on topology optimization. *Journal of Mechanical Design* **2018**, *140*, 091403.
4. Larsen, S.; Sigmund, O.; Groen, J. Optimal truss and frame design from projected homogenization-based topology optimization. *Structural and Multidisciplinary Optimization* **2018**, *57*, 1461–1474.
5. Sokół, T. Topology optimization of large-scale trusses using ground structure approach with selective subsets of active bars. In Proceedings of the 19th International Conference on Computer Methods in Mechanics. Warsaw, Poland, 2011.
6. Ohsaki, M. *Optimization of finite dimensional structures*; CRC Press, 2016.
7. Sanders, E.D.; Ramos Jr, A.S.; Paulino, G.H. A maximum filter for the ground structure method: an optimization tool to harness multiple structural designs. *Engineering Structures* **2017**, *151*, 235–252.
8. Ghoddosian, A.; Vezvari, M.R.; Azqandi, M.S.; Karimi, M.A. Topology optimisation of the discrete structures with the minimum growing ground structure method. *International Journal of Structural Engineering* **2018**, *9*, 38–49.
9. Li, Z.; Luo, Z.; Zhang, L.C.; Wang, C.H. Topological design of pentamode lattice metamaterials using a ground structure method. *Materials & Design* **2021**, *202*, 109523.
10. Ranalli, F.; Flager, F.; Fischer, M. A Ground Structure Method to Minimize the Total Installed Cost of Steel Frame Structures. *International Journal of Civil and Environmental Engineering* **2018**, *12*, 160–168.
11. Habte, B.; Yilma, E. Cost optimization of reinforced concrete frames using genetic algorithms. *An International Journal of Optimization and Control: Theories & Applications (IJOCTA)* **2021**, *11*, 59–67.
12. Alkam, F.; Lahmer, T. Quantifying the Uncertainty of Identified Parameters of Prestressed Concrete Poles Using the Experimental Measurements and Different Optimization Methods. *Appl. Sci* **2019**, *4*, 84–92.
13. Esfandiari, M.; Haghighi, H.; Urgessa, G. Machine learning-based optimum reinforced concrete design for progressive collapse. *Electronic Journal of Structural Engineering* **2023**, *23*, 1–8.
14. Liu, F.; Yang, H.; Gardner, L. Post-fire behaviour of eccentrically loaded reinforced concrete columns confined by circular steel tubes. *Journal of constructional steel research* **2016**, *122*, 495–510.
15. Zhu, Y.; Yang, H.; Gardner, L.; Wan, J. Performance of reinforced concrete-filled steel tubular (RCFST) members subjected to transverse impact loading. *Journal of Constructional Steel Research* **2022**, *188*, 107018.
16. Zegard, T.; Paulino, G.H. GRAND—Ground structure based topology optimization for arbitrary 2D domains using MATLAB. *Structural and Multidisciplinary Optimization* **2014**, *50*, 861–882.
17. Tsiptsis, I.N.; Liimatainen, L.; Kotnik, T.; Niiranen, J. Structural optimization employing isogeometric tools in Particle Swarm Optimizer. *Journal of Building Engineering* **2019**, *24*, 100761.
18. Elbes, M.; Alzubi, S.; Kanan, T.; Al-Fuqaha, A.; Hawashin, B. A survey on particle swarm optimization with emphasis on engineering and network applications. *Evolutionary Intelligence* **2019**, *12*, 113–129.
19. Sigmund, O. A 99 line topology optimization code written in Matlab. *Structural and multidisciplinary optimization* **2001**, *21*, 120–127.

 doi:10.20944/preprints202604.0258.v1

20. Behrou, R.; Lotfi, R.; Carstensen, J.V.; Ferrari, F.; Guest, J.K. Revisiting element removal for density-based structural topology optimization with reintroduction by Heaviside projection. *Computer Methods in Applied Mechanics and Engineering* **2021**, *380*, 113799.
21. Lazarov, B.S.; Wang, F.; Sigmund, O. Length scale and manufacturability in density-based topology optimization. *Archive of Applied Mechanics* **2016**, *86*, 189–218.
22. Gaynor, A.T.; Guest, J.K.; Moen, C.D. Reinforced concrete force visualization and design using bilinear truss-continuum topology optimization. *Journal of Structural Engineering* **2013**, *139*, 607–618.
23. Changizi, N.; Jalalpour, M. Stress-based topology optimization of steel-frame structures using members with standard cross sections: gradient-based approach. *Journal of Structural Engineering* **2017**, *143*, 04017078.
24. Olsson, A.; Sandberg, G.; Dahlblom, O. On Latin hypercube sampling for structural reliability analysis. *Structural safety* **2003**, *25*, 47–68.
25. Kirkley, A.; Barbosa, H.; Barthelemy, M.; Ghoshal, G. From the betweenness centrality in street networks to structural invariants in random planar graphs. *Nature communications* **2018**, *9*, 2501.
26. Zheng, L.; Karapiperis, K.; Kumar, S.; Kochmann, D.M. Unifying the design space and optimizing linear and nonlinear truss metamaterials by generative modeling. *Nature Communications* **2023**, *14*, 7563.
27. Standard, B. Eurocode 2: Design of concrete structures—. *Part 1* **2004**, *1*, 230.
28. Kim, H.; Querin, O.; Steven, G.; Xie, Y. A method for varying the number of cavities in an optimized topology using evolutionary structural optimization. *Structural and Multidisciplinary Optimization* **2000**, *19*, 140–147.